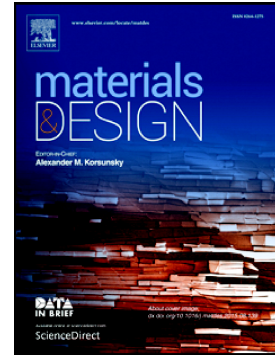# Accepted Manuscript

Salt-metal feedstocks for the creation of stochastic cellular structures with controlled relative density by powder bed fabrication

G. Zhao, I.A. Ashcroft, R.J.M. Hague, A.R. Kennedy, A.T. Clare

Please cite this article as: G. Zhao, I.A. Ashcroft, R.J.M. Hague, A.R. Kennedy, A.T. Clare , Salt-metal feedstocks for the creation of stochastic cellular structures with controlled relative density by powder bed fabrication. The address for the corresponding author was captured as affiliation for all authors. Please check if appropriate. Jmade(2017), doi:10.1016/j.matdes.2018.03.071

Salt-metal feedstocks for the creation of stochastic cellular structures with controlled relative density by powder bed fabrication

[a]G. Zhao, [a]I. A. Ashcroft, [a]R. J. M. Hague, [b]A.R. Kennedy, [a]A.T. Clare

[a]Faculty of Engineering, The University of Nottingham, Nottingham, NG7 2RD, U.K.

[b]Engineering Department, Lancaster University, Lancaster, LA1 4YW

Abstract

A novel type of metallic feedstock material for powder-bed additive manufacturing (AM) processes is proposed that enables the manufacture of cellular structures without the time consuming and computationally intensive step of digitally representing the internal geometry of a part. The feedstock is a blend of metal and salt particles and, following Selective Laser Melting (SLM) processing, the salt is dissolved to leave a metallic, cellular structure. The conditions for succesfully processing the feedstock are first demonstrated, followed by an investigation into how the feedstock composition can be used to control the relative density of the cellular material. Mechanical testing reveals that the strength and stiffness of the cellular structures can be tuned through control of feedstock composition, and hence, relative density. This presents a significant enhancement to the state-of-the-art for materials preparation for AM since, for the first time, cellular structures can be created with specific properties without explicitly defining or analysing the unit cell geometry.

Keywords

Additive manufacturing, selective laser melting, cellular structures, porous structures

1. Introduction

Cellular materials are commonly found in nature in both regular and irregular (or stochastic) arrays. The advantages of such structures, including high specific strength and weight, have been exploited in engineered analogues, such as honeycomb and foamed metal structures. For example, sandwich panels with foamed or honeycomb titanium cellular cores are used as structural materials for aerospace engineering, due to their low densities, high melting temperature and excellent mechanical properties [1]. They have also been developed as implant materials as they show good compressive properties and often exhibit excellent biocompatibility when appropriate alloys are used [2]. Furthermore, the compressive strength and modulus of titanium foams can be adjusted through the control of pore size, strut thickness and relative density [3].

Traditional methods to fabricate cellular Ti structures include reactive sintering [4], hollow sphere sintering [5], loose powder sintering [6] and 'space holder' techniques, which require a dissolution procedure [7]. Among these powder metallurgy techniques, the 'space holder technique' has attracted significant attention since it offers the ability to control pore size, shape and distribution [8]. Magnesium [9], Carbamide [10, 11], NaCl [12, 13] and Acrowax [14] have all been used as space holders in the literature. However, a major drawback to the more general adoption of these materials is that current methods of Ti cellular structure manufacture present significant limitations, such as multiple process steps and the production of geometries which are limited by the mould tooling complexity. Furthermore, removal of the space-holder without surface residue and deleterious effects upon the near surface metallurgy are critical concerns when selecting materials for this purpose.

Additive Manufacturing (AM) enables the manufacture of complex structures without the

need for sophisticated tooling or multiple processes. AM techniques, therefore, have the potential to remove many of the limitations associated with current cellular structure manufacture, such as greater control over cell type, density and grading, incorporation into solid structures in a single step and conformance to complex external geometries. One of the most popular AM methods for industrial application is selective laser melting (SLM), which makes use of a scanning laser to melt metal powders layer-by-layer in an inert gas atmosphere. Processing of titanium and the production of titanium alloy lattice structures using SLM is well established [15, 16]. However, the manufacture of lattice and cellular type structures within SLM requires the explicit design, analysis and optimization of complex geometries. This is extremely challenging, in terms of computational methods and computer resources.

In this paper, a new method, combining SLM with a space-holder technique is demonstrated that is able to build cellular Ti-6Al-4V parts without the explicit design stage. The relative volume fractions of space-holder and metal powders (in this case NaCl and Ti-6Al-4V, respectively), were investigated to achieve cellular structures with a range of relative density, and hence mechanical properties. The purpose of this study is to demonstrate that SLM can be used to rapidly create porous structures without the need for complex analysis to define the geometry in a deterministic fashion. This represents a significant enhancement to the-state-of-the-art through the creation and characteriation of a new family of feedstock materials for SLM.

2. Materials & Methodology

2.1 Experimental Material

Plasma-atomized, spherical Ti-6Al-4V powder (ASTM B348, LPW Technology Ltd.,

Cheshire, UK) with a mean particle size of ~35 μm and sodium chloride (NaCl-98% purity) powder with a mean size of ~150 μm were used as the lattice material and space holder respectively. The composition of the Ti-6Al-4V powder is shown in Table 1.

Table 1 Composition of the Ti-6Al-4V as supplied by LPW

	Ti (wt. %)	Al (wt. %)	V (wt. %)	Fe (wt. %)	O (wt. %)
Nominal	Balance	5.5-6.5	3.5-4.5	<0.25	<0.13

The morphology and size distribution of the two materials is shown in Figure 1. The particle size distribution was determined using a Malvern UK Mastersizer 3000, which uses laser diffraction to measure the size of particles through measuring the intensity of light scattered as a laser beam passes through a dispersed particulate sample. The morphology of Ti-6Al-4V was characterised using a Philips XL30 scanning electron microscope (SEM), and the NaCl powder was viewed with a Nikon Eclipse LV100ND optical microscope. It can be seen in Figure 1 that the NaCl particles are cubic in shape, compared to the much smaller, spheroidal Ti-6Al-4V powder. This increases the probability that the finer Ti-6Al-4V powders will surround the coarser NaCl powders when they are mixed to form a continuous lattice structure, as desired.
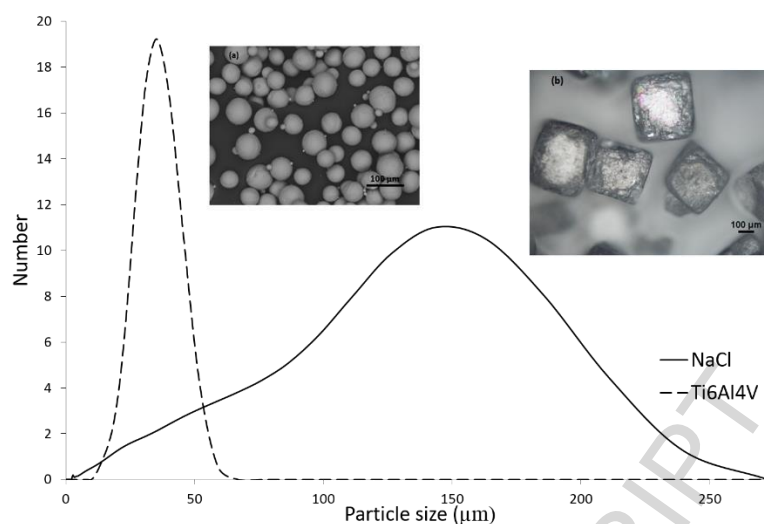
Figure 1. Morphology and particle size of (a). Ti-6Al-4V particles; (b). NaCl powders

The thermal properties including melting temperature, evaporation temperature and thermal conductivity of both materials are shown in Table 2. It is notable that the boiling temperature of the salt is lower than the melting temperature of the metal, indicating that at least some vaporisation of the salt may be expected during processing if the metal is melted. Furthermore, the thermal conductivity of the salt is significantly lower than that of the metal at typical processing temperatures, hence, localised heat would be expected to flow through the metal in preference to through the salt.

Table 2 Thermal properties of Ti-6Al-4V and NaCl after Nagasaka et al. [17] and Boiveneau et al. [18]

| Material	Melting temperature (°C)	Boiling temperature (°C)	Thermal conductivity (W/(m·°C))
Ti-6Al-4V	1604-1660		15 at 1200°C 20 at 1400°C
NaCl	801	1413	0.5 at 1170°C 0.45 at 1400°C

2.2 Powder Mixing

In order to produce samples with a range of relative densities in the final structure, feedstocks of various volume ratios of NaCl: Ti6Al4V were prepared. In the first step, 300g of Ti-6Al-4V powder was hand-mixed with NaCl for 2-3 minutes, with NaCl proportions varying from 10% to 60 vol. %. Following this, the blends were mixed in a gyroscopic mixer for 30 minutes. The powder mixes were dried in an oven before use. Figure 2 shows a 50 vol. % NaCl mixture. The NaCl and smaller, more spherical Ti-6Al-4V particles can be clearly differentiated. Some of the NaCl particles appeared to cleave during mixing and as a result smaller NaCl crystals are observed in the mixture. It may be expected that the range of salt crystal sizes would result in a corresponding range in lattice cell sizes in the processed material. This is not investigated explicitly in this work but clearly the potential to control the stochasticity of the cellular structure through control of the space holder (in this case NaCl) size distribution exists.
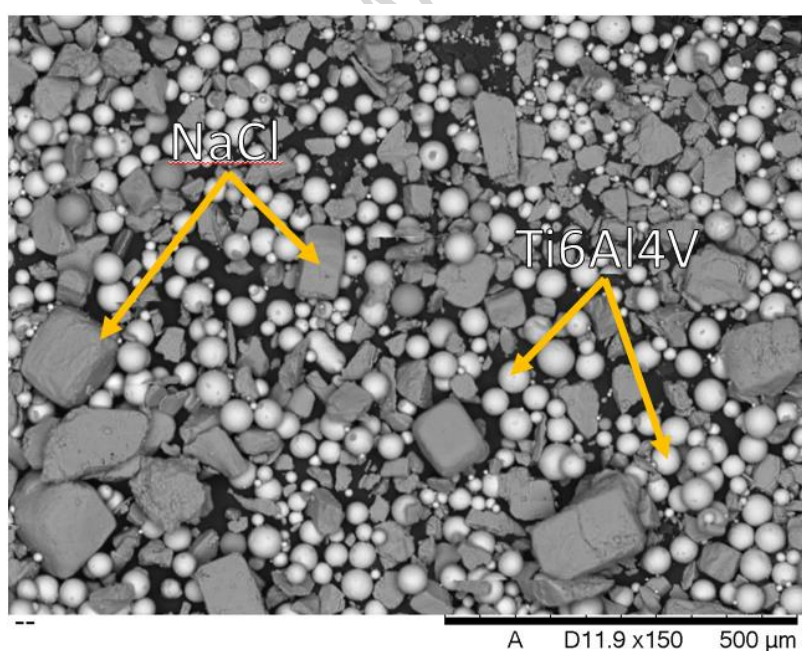
Figure 2. Exemplar blend of 50% mixture by volume. Salt and metal constituents can be clearly observed

One of the important considerations in using such a mixed feedstock is that the resulting powder mix retains sufficient flowability to enable the feed and spreading mechanisms in the

particular SLM machine used to deliver a uniform and compact powder layer. The flowabilities of the mixed feedstocks were evaluated using a hall flow test according to ASTM B213. Figure 3 shows the relationship between NaCl content and the time needed for 50g mixtures of powder to flow through the orifice. It can be seen that time increased, i.e. flowability decreased, linearly with increasing NaCl content. Poor flowability is known to lead to an uneven distribution of powder, which can result in build defects. However, in this case, even though flowability decreased with increasing salt content, the powder distribution system was able to deliver a visually compact and even powder bed within the salt content range of interest. Even so, it should be borne in mind that with the proposed technique, this is a factor that requires careful consideration when selecting the size and shape distributions of the matrix and space holder powders.
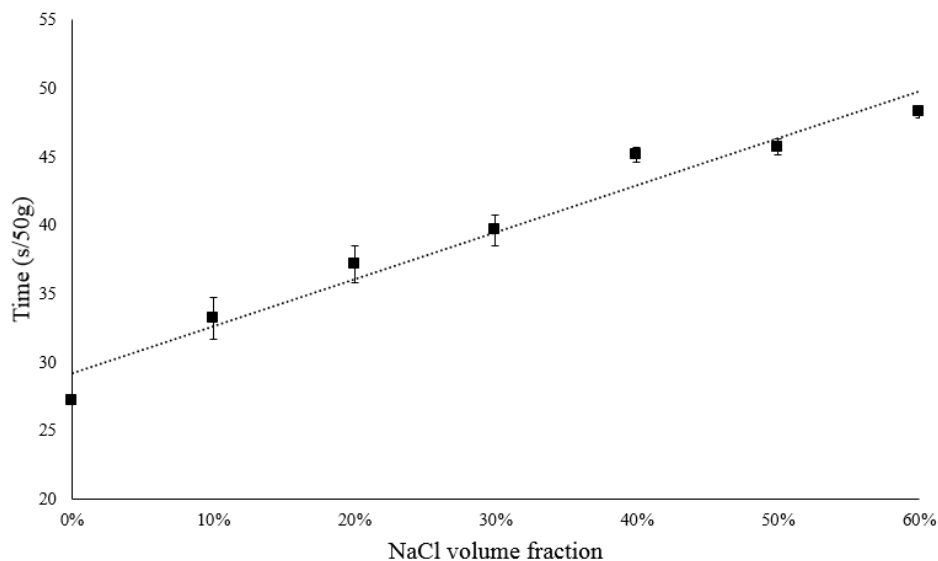
Figure 3. Hall flow test results as a function of salt content in the mixed powder feedstock.

This figure clearly shows that the addition of NaCl to this feedstock increases the time take for the blend to exit the orifice. This is a broad indicator of flowability, however, flow conditions are well known to be different within powder bed feed mechanisms where temperature and hopper conditions are important factors. Mellin et al. [19] have reported on

the evaluation of flowability for powder bed processes and have related simple techniques to powder bed formation.

2.3 Selective Laser melting (SLM)

SLM processing was carried out using a Realizer Gmbh SLM-50, Germany, equipped with a 100 W Yttrium fibre laser. 5 mm cubic specimens were built on a titanium alloy substrate in an argon gas atmosphere of less than 1% oxygen content. The SLM system was operated in its normal mode with the feedstock delivered from a standard hopper and conventional wiper arrangements were utilised. Figure 4 shows a schematic of the process used to create the cellular structures, in which leaching of the space holder material succeeds the SLM stage.

A double scan strategy, in which each layer was scanned in both X and Y directions was employed, with a layer thickness of 45 μm and hatch spacing of 60 μm, based on previous studies for the processing of titanium powders [20]. The effects of laser power and scan speed were investigated, with power ranging from 10W to 100W and scan speeds from 100 mm/s to 300 mm/s. The build platform was held at 200°C throughout fabrication. Laser energy density (E) is considered to be a crucial factor affecting the properties of fabricated parts in the SLM process. It is defined in Equation (1), where P is laser power (W), v is scan speed (mm/s), h is hatch spacing (mm) and t is layer thickness (mm).

$$E = \frac{P}{v \times h \times t} \qquad (1)$$

2.4 Salt Dissolution

Fabricated cubes were placed in water at room temperature in order to leach out the NaCl. In initial trials the cubes were removed from the water, dried and weighed periodically until the weight of the cubes was stable, at which point it was assumed that all unbound NaCl had been removed from the cube. The final weight of cubes after removal of the NaCl was used to

determine the density of the lattice structure. The weight of the cubes were measured using an

ABT100-5M (Kern &Sohn GmbH, Germany) analytical balance.
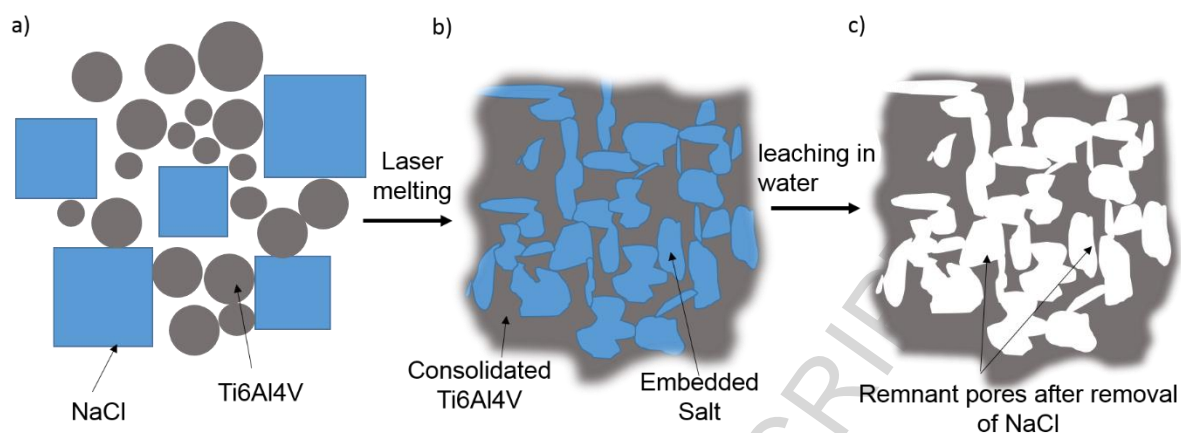
Figure 4. Schematic of the process creating cellular structures. a) The powder bed consists of both Ti6Al4V powder and larger NaCl particles. b) Following laser consolidation metal flows around the salt inclusion but connectivity is retained for a successful parameter set c) A leaching procedure removes the salt and a porous structure results. Noting full removal will only take place with sufficiently high connectivity between NaCl particles.

2.5 Characterisation of Meso and Microstructure

In order to characterize the cellular structures created by SLM of the combined metal-salt feed material, test samples were prepared for analysis by sectioning, mounting, grinding and polishing. The microstructure was studied using both optical microscopy and scanning electron microscopy (SEM). Composition of the samples was assessed using energy dispersive spectroscopy (EDX) in the SEM. The meso-structure of the samples, here defined as the structure on the scale of the individual lattice cells, was characterized by micro-focus X-ray computed tomography (micro-XCT). XCT data processing was performed using the public domain image processing software ImageJ. Each XCT measurement provided a stack of images, each representing a cross-section in the xy plane with a layer thickness of 7.16 µm. A sample of 100 images, equally spaced throughout the vertical direction of the specimen, was taken to expedite the analysis procedure. The densities of each cube was calculated from

the measured weight and volume of each sample. The volume was determined from physical dimensions measured by vernier caliper.

2.6 Mechanical Testing

Compression testing to evaluate yield strength and modulus was carried out using samples of approximately 5 x 5 x 5 mm^3. Samples were tested using an Instron 5969 universal testing machine at room temperature with a strain rate of 10^{-3} s^{-1}. For each specimen type, five repeat tests were carried out. In the calculation of stresses, the sample cross section was used rather than the actual material cross section, which varied with relative density of the cellular structure Hence lattice, rather, than bulk properties were generated.

3 Results

3.1 Optimisation of Processing Parameters

The energy density for each SLM parameter set was calculated from Equation (1). The resulting processing map is shown in Figure 5. Energy density is shown to have a marked effect on the properties of as-built parts. For example, when lower than 50 J/mm^3, there is insufficient heat to melt and flow titanium powders at 10 and 20 vol. % NaCl. By increasing NaCl content, less energy is needed for sample fabrication due to the lower localised mass required for melting. At the other extreme, if the input energy is excessive, for example, when energy density exceeds 100 J/mm^3 for 50 and 60 vol. % NaCl, excessive evaporation leads to the failure of fabrication. The optimum energy density at each NaCl volume fraction varies with salt content. With 10 to 30 vol. % NaCl, the majority of the parameter sets investigated were able to successfully build parts. However with 60 vol. %, a limited range of parameters with low energy density is successful. In subsequent experiments processing parameters used to fabricate cubes were selected from the process map shown in Figure 5.
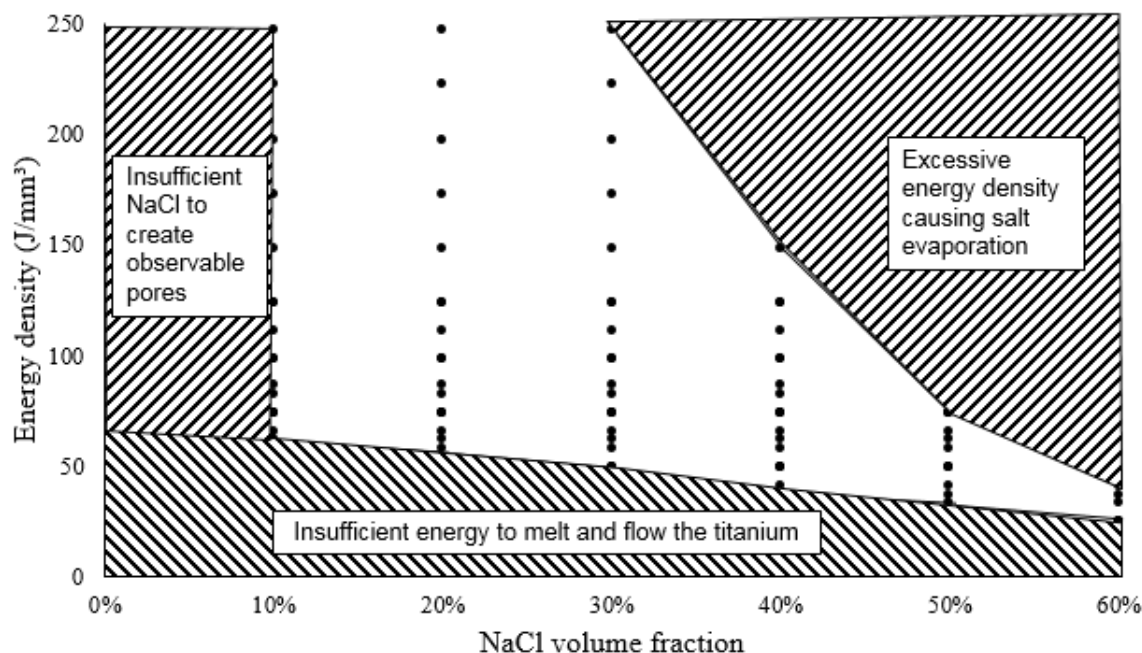
Figure 5. Processing map of mixtures with various NaCl content

3.2 Salt dissolution

Figure 6 presents the salt dissolution rate of each cube with varying NaCl content. As the volume fraction of NaCl in the initial powder state increases, the as-fabricated weight of the cubes decreases from ~0.60 g (at 10 vol. % NaCl) to ~0.37 g (at 60 vol. % NaCl). After dissolving in water for 10 minutes, the weight remains constant for all cubes. As would be expected, it can be seen that the initial rate of NaCl removal, as well as total amount removed, increased with the percentage of salt crystals in the feedstock. It should be noted that the amount of salt removed from the built part was less than that calculated based on the initial volume fraction of the feedstock. This is because some of the salt is evaporated during processing, as indicated by table 2, and discussed further in section 3.5. It was also seen that at low volume fractions of salt, residual NaCl could be seen to be trapped in the built sample, as discussed further in the next section.
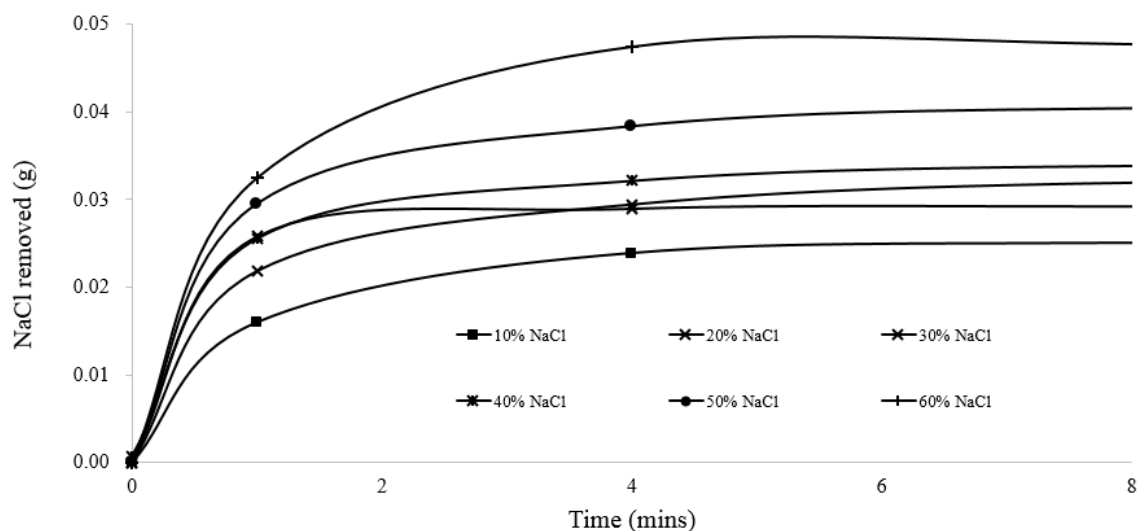
Figure 6. Salt dissolution as measure by the change in specimen mass with time

3.3 Characterisation of the cellular structure

Sections of the 5 mm cubes with NaCl volume fraction from 10% to 60% are presented in Figure 7. It is observed that with increasing NaCl volume fraction in the feedstock, the volume fraction of voids in the built structure increased, or in other words, the relative density of the lattice structure decreased. The structure developed from a closed-cell at low volume fractions of NaCl in the feedstock to a more inter-connected, and finally to an open-cell foam-like structure, as salt content in the feedstock increased. The pores in this process are irregular in shape and size compared with traditional space holder sintering techniques. Analysis of pore volume indicated that at low salt content, pores tended to be smaller than the salt particles in the initial feedstock but at high volume fractions of salt, pore size tended to be larger than the salt particles. The observed structures can be attributed to a number of influences. The sintering of Ti alloys can occur at a lower temperature, 720 °C for instance [21], than the melting temperature of NaCl, 801 °C, however, full melting of Ti6Al4V occurs above the boiling point of the NaCl. From this we may deduce that during processing some

12

salt evaporates, resulting in there being less salt (and hence) pores in the built structures than in the feedstock and also accounting for the pores being smaller than the salt particles at low salt volumes. It is also notable that the thermal conduction of the Ti6Al4V is an order of magnitude greater than that of the salt at typical processing temperatures, hence, heat will tend to flow preferentially through the consolidated metal, resulting in some of the salt either remaining solid or melting and solidifying, the latter accounting for the change in morphology of the pores. Furthermore, it is proposed that the pores that are greater in size are formed by agglomerations of salt particles, either from the powder bed distribution or from salt melt-solidification during processing.
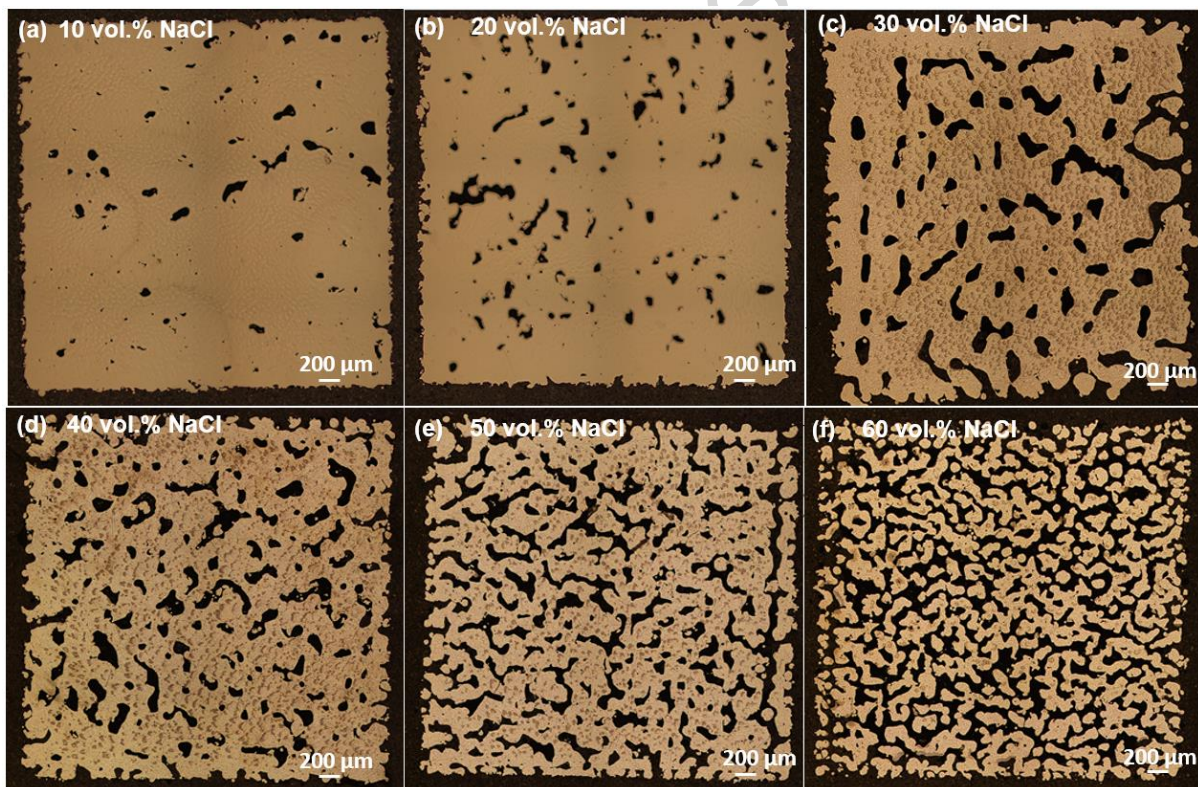

Figure 7. Optical micrograph sections in the x-y plane showing the pore distribution within cubes with varying volume fraction of NaCl at (a) 10%; (b) 20%; (c) 30%; (d) 40%; (e) 50%; (f) 60%.

3.4 Characterisation of Microstructure

Figure 8 shows a comparison between a typical pure Ti-6Al-4V microstructure and a region

around a pore in a 30 vol. % NaCl specimen. Ti-6Al-4V transforms fully into the β phase field above the β transfer temperature (~ 950°C) and into an α+β phase mixture below this critical temperature [22]. The amount of β phase retained at room temperature is governed by the cooling rate experienced from the β phase field. During SLM, each layer cools rapidly thus the microstructure is dominated by the martensitic (α′) phase. In Figure 8 (a), a complete martensitic structure can be observed. In Figure 8 (b), complete α′ phase is still clearly seen in the metal in close proximity to the pore. It can, therefore, be concluded that there is no significant metallurgical effect due to the proximity of NaCl during processing of the mixed feedstock.
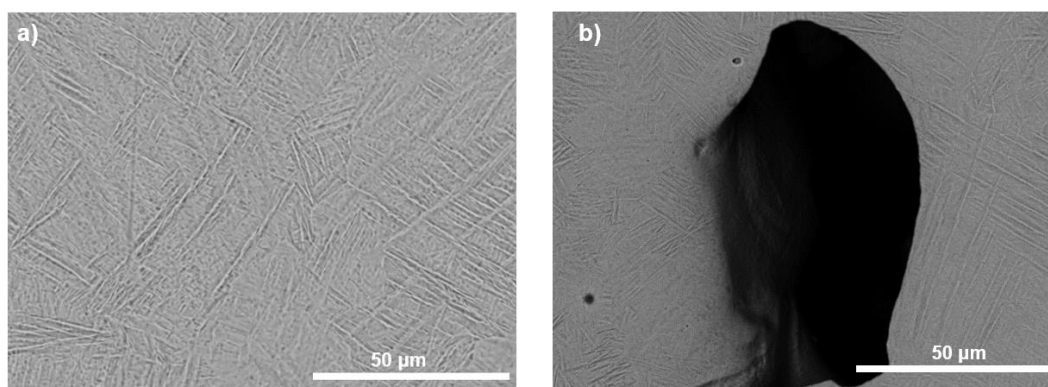
Figure 8. Metallurgy comparison between (a) cube without NaCl and (b) cube with 30 vol. % NaCl

In order to determine the degree of diffusion of NaCl into the bulk of the porous structure EDX was undertaken. Two regions were investigated which were evaluated using elemental mapping techniques. This can be observed in Figure 9. The contribution to the bulk metallurgy of the resulting material is shown to be minimal.

Spectrum	Na (weight.%)	Cl (weight.%)
1	0.13	0
2	0.06	0
3	0.01	0
4	0.01	0
5	0.08	0
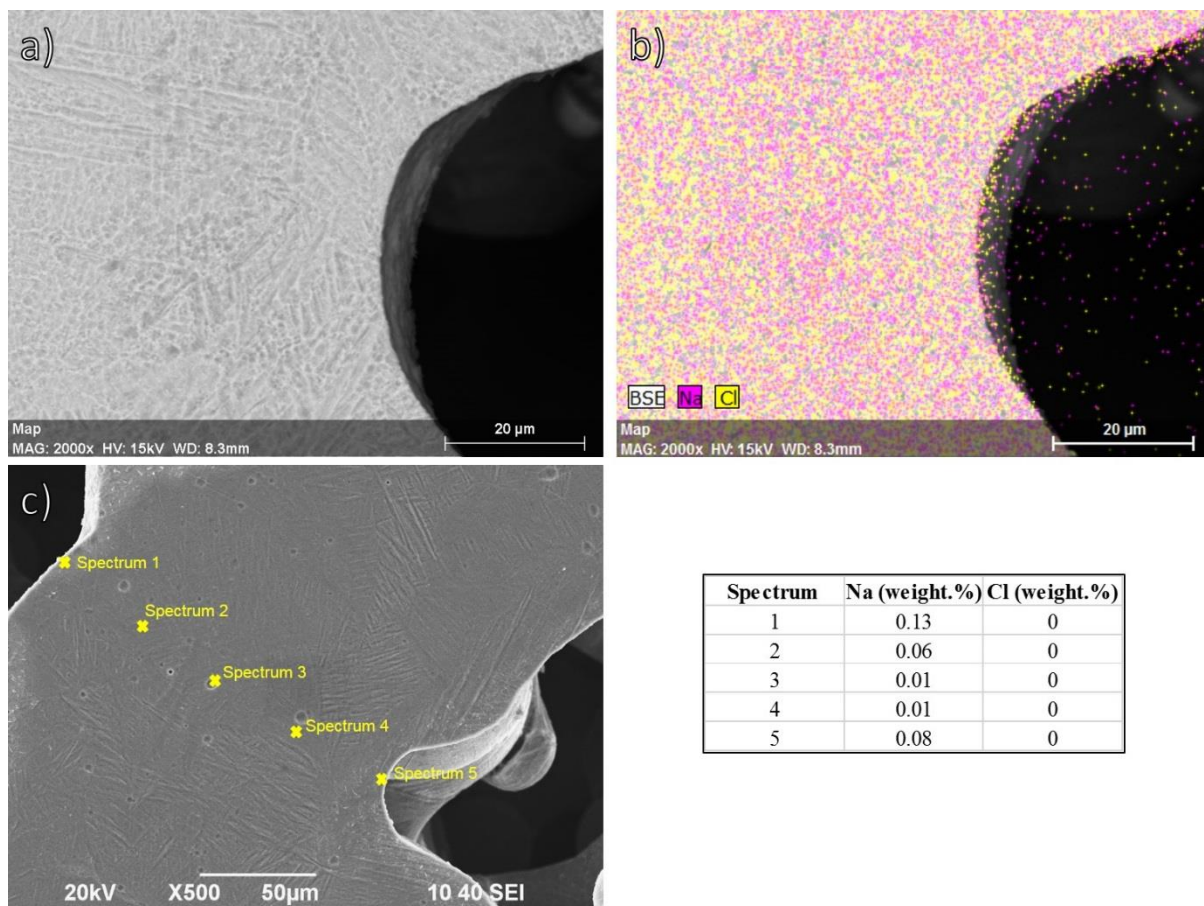
Figure 9. The contribution of Na and Cl to the elemental composition of the porous structure is minimal. b) shows an elemental EDX map of the micrograph shown in a). c) and the inset table show the distribution of Na within the solid as minimal. Cl was not detected here.

Concentration of Na and Cl is not observed to be markedly higher at the near surface but point analysis (Figure 9c) shows that Cl was not detected under the evaluation conditions detailed here. It is clear that the selection of space holder material can a have a critical role in the morphology of the resultant material but in this case a minimal effect on metallurgy is observed.

3.5 Relationship between feedstock composition and relative density

The relative density (ρ_r) of a lattice (or cellular) structure is defined as the ratio of the density of the lattice structure (ρ_f) and the density of the solid material (ρ_s), as defined in Equation 2. Figure 9 illustrates the relationship between NaCl volume fraction and the relative density of the cellular structures created from the mixed feedstock method.

$$\rho_r = \frac{\rho_f}{\rho_s} \qquad\qquad (2)$$

Increasing NaCl content in the feedstock is shown, as expected, to cause a systematic increase in porosity and corresponding decrease in relative density. Assuming zero evaporation or dissolution of the NaCl, the porosity volume would equate to the NaCl volume fraction. In practice the relative density is higher than would be predicted with this assumption, indicating some NaCl evaporation takes place. In addition where NaCl is entirely encapsulated it will not be removed by leaching. It can be seen that the relationship between NaCl volume fraction and relative density is quite linear over a significant range but deviates at high relative density to meet the boundary condition of relative density equal to 1 at 0% NaCl. The equation displayed in the figure gives the relationship between NaCl volume fraction and actual relative density in the linear region, which also corresponds to the range in which useful cellular structures are seen, as will be demonstrated in the next section. This can be used to predict the experimental porosity and relative density of fabricated samples taking the above caveats into consideration.
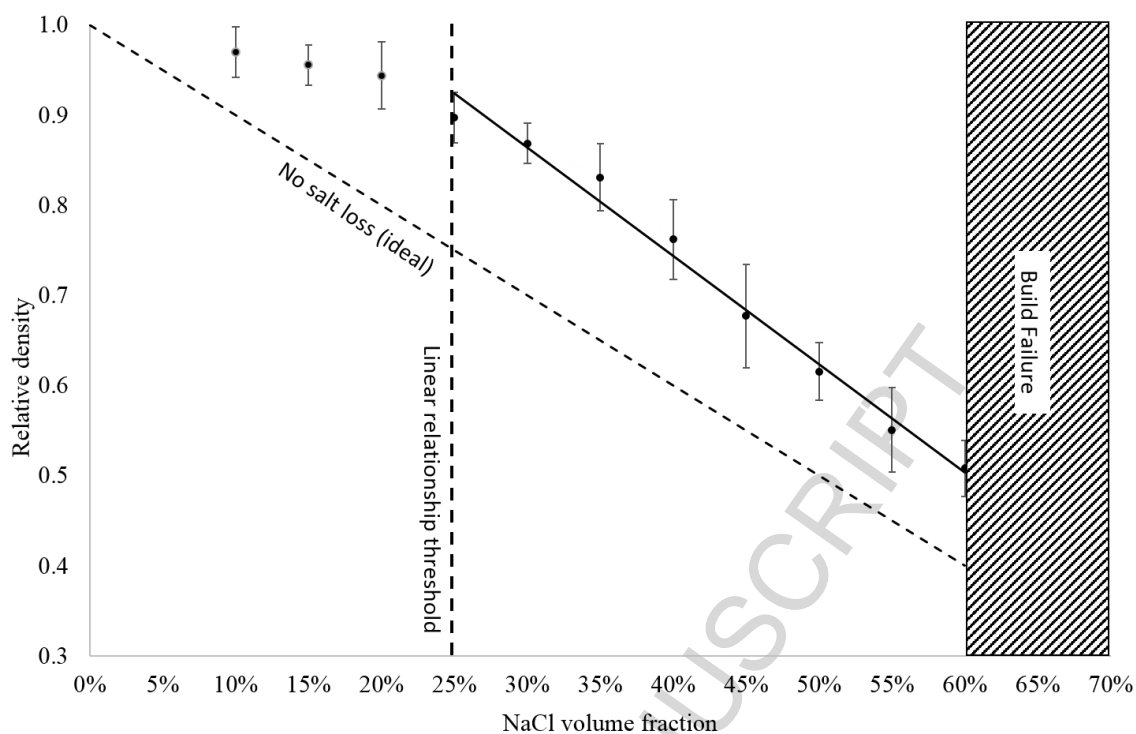
Figure 10. The experimentally obtained relative density showing the uniform error across salt content within the feedstock. Equation for the linear region is given by $\rho_r = -1.2016X + 1.2245$ where X is the NaCl volume fraction. XCT was used to calculate the relative density here

3.6 Mechanical Testing

Figure 10 presents the stress-strain compression curves of the 5 mm cubes with various NaCl volume fractions. As expected, compressive yield strength and modulus of the lattices were observed to decrease with increasing NaCl content. Figure 11 shows images of two cubes with 30 vol. % NaCl and 60 vol. % NaCl respectively during compression testing. All specimens show an initial region in which full contact is made followed by a linear elastic region. As load is increased beyond this region, plastic deformation occurs, followed by cracking. This sequence is indicative of the brittle nature of the as-built material, as it may be expected with a ductile material that rather than cracking, the behaviour under high loads would feature an increasing load as plastic deformation leads to contact and compaction of the lattice. The brittle behaviour observed here is typical of the as built condition of high

strength metals manufactured by SLM, however, ductility can often be recovered in these

materials by a suitable heat treatment.
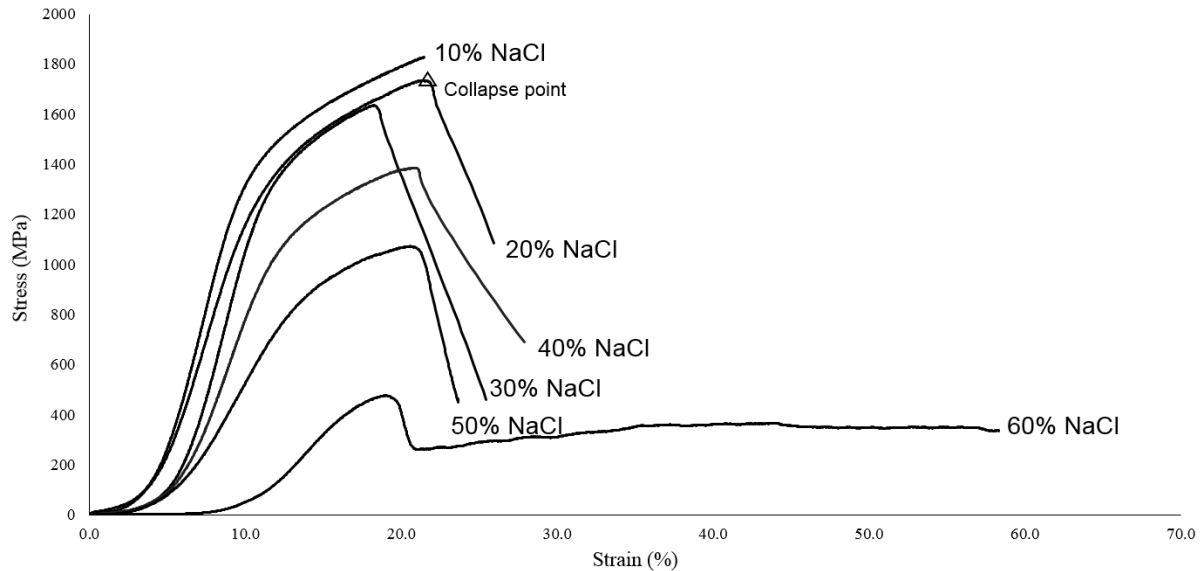
Figure 11. Effect of salt content on mechanical properties in compression demonstrated by the characteristic stress-strain relationships

It was seen in Figures 9 and 10 that relative density of the cellular structures created and the

subsequent mechanical properties where dependent on the volume fraction of salt in the

feedstock. In fact, a more useful correlation is between the relative density and mechanical

properties of the lattice strcture, as presented in Figure 12. In this figure Region 1 indicates an

open cellular structure type response and Region 2 denotes semi-solid structures with a

population of isolated pores. It is Region 1 that is of interest in terms of usful lattice structues

and it is instructive to compare the mechanical response in this region to Equations (3) and

(4) proposed by Gibson and Ashby [23]. The coefficients C_1 and C_2 were determined by

Gibson and Ashby to be approximately 0.3 and 1.0 respectively from a study of metal foam

data [23].

$$\frac{\sigma^*}{\sigma_s} = C_1 (\frac{\rho^*}{\rho_s})^{3/2} \qquad (3)$$

$$\frac{E^*}{E_s} = C_2 (\frac{\rho^*}{\rho_s})^2 \qquad (4)$$

Relative compressive strength and relative compressive modulus were evaluated in this study. Since processing parameters were optimised for salt integration and not the fabrication of solid builds comparison with wrought (114 Gpa) [24] or even optimised compressive moduli through SLM was not appropriate. In this case a specimen was produced with zero salt addition at the laser parameters used for the 10 vol. % NaCl composition. This was found to be 25.9 GPa and was thus considered to be the modulus of a solid specimen which was used to normalise compressive moduli data. In Figure 12, it can be seen that in Region 1 both the compressive strength and modulus decrease with decreasing relative density. The experimential data indicates a slightly non-linear relationship between relative density and relative compressive properties in Region 1. Fitting equations of the form of Eqns. (3) & (4) results in a proportionality and exponent constants of 1.13±0.06 and 1.58±0.15, respectively, for the yield strength, and 0.06±0.01 and 2.41±0.33, respectively, for the compressive modulus. The theoretically calculated values of the exponent constants in Eqns. (3) & (4) are based on the mechanics of open cell foams as represented by a regular cubic array of square sectioned members. Whilst this model has been shown to be generally applicable to equiaxed open cell foams, this is far from the case with the cells produced here, which may account for the difference in the values of the constants from those proposed by Gibson and Ashby. However, the forms of equations (3) and (4) fit the data well in Region 1 and the experimentally determined constants can be used to predict properties based on salt content of the feedstock to a fair degree of accuracy.

In Region 2, with relative density above approximately 0.8, the relative compressive yield

strength and modulus fluctuate around 0.97 and 0.9 respectively. In this region it is best to consider the structure as that of a solid with a population of isolated pores.
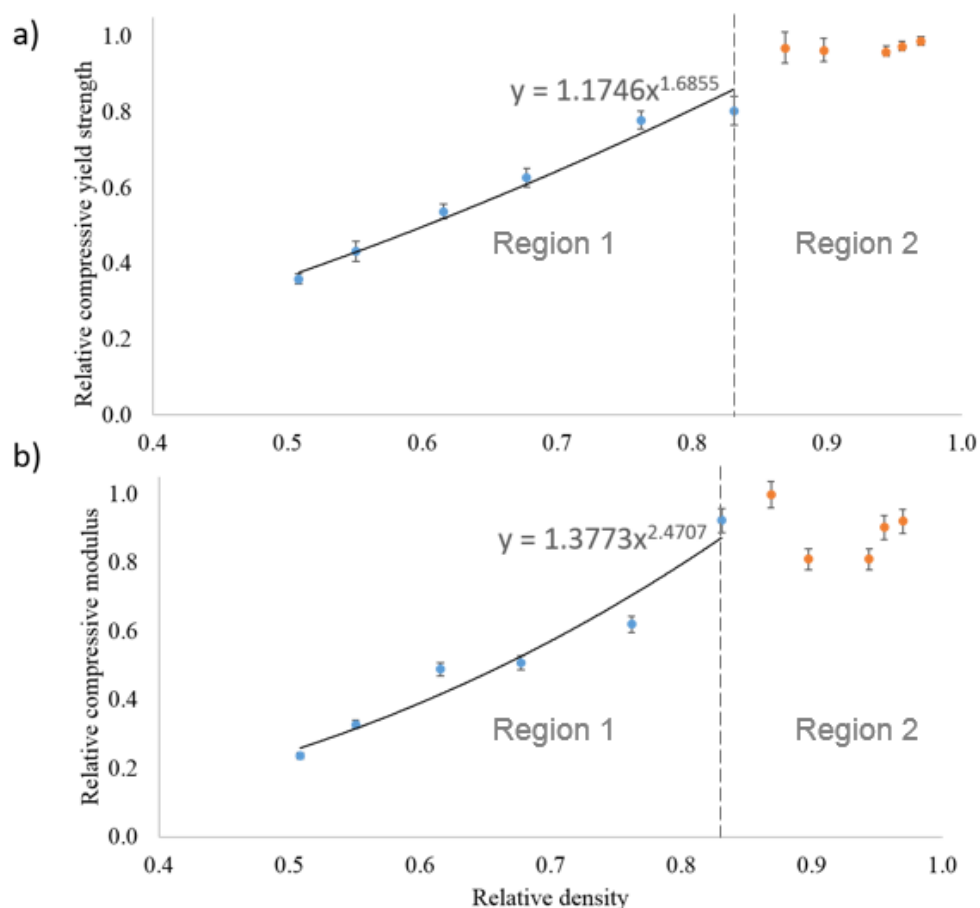
Figure 12. Relationship between cube relative density and compressive properties. Error bars result from the standard deviation of 5 compression test and three density measurements per specimen. a) Shows specimen relative compressive yield strength and b) shows relative compressive modulus normalised by compressive modulus of 100% Ti6Al4V built using parameters optimised for salt inclusion (*see* Section 3.1)

4. Discussion

A novel feedstock preparation for SLM using a blend of Ti-6Al-4V and NaCl has been demonstrated. The technique relies upon the fabricated parts being placed in water to enable removal of the remaining NaCl after processing through the open porosity generated, leaving the structure as a metallic part with a cellular, or lattice, structure. To achieve such a structure

requires a sufficient level of connectivity between the space holding material to allow removal by leaching. Cross sectional analysis of specimens produced in this way, shown in Figure 7, suggests that there is low connectivity in structures below 30% vol. NaCl, with some NaCl subsequently trapped within the structure, even after the leaching procedure. In addition, due to the working temperature of the SLM process when processing Ti being typically higher than the boiling point of NaCl, some NaCl particles may partially or completely evaporate during the process. Liquid phase flow of the NaCl in process is also evident from the resulting pore morphology. For all specimens presented in this study pores are rounded and anisotropic in shape, which is in clear contrast to the angular cubic geometries characteristic of the input NaCl crystals shown in Figure 1.

A range of processing parameters were explored in order to accommodate a wide range of Ti-6Al-4V:NaCl feedstocks, as reported in Figure 5. According to this processing map less energy is needed with higher NaCl content in the mixture since there is a lower volume of localised Ti-6Al-4V which must be melted in order to consolidate the part.

According to the equation in Figure 9, the relative density of a fabricated part can be predicted based on the composition of the feedstock. This presents a useful design guide in order to modulate porosity uniformly without the need for complex fabrication strategies to be defined.

The traditional furnace-based sintering and space holder technique presents significant limitations when compared to this approach. Furthermore, functionally graded structures may be achievable by controlling the NaCl content in one part, using the equation for prediction of densities at each subsection without any explicit design, analysis and optimization, reducing the computational design and analysis overhead compared with deterministic lattice structures produced by SLM process.

Compared with the traditional sintering process and SLM fabricated lattices, the pore size,

shape and distribution from this process is stochastic, therefore the mechanical properties, for example, the compressive modulus and yield strength do not closely fit to Gibson and Ashby's equation of foam structures. It is therefore necessary to investigate the relationship between processing parameters and structures in future work such that the properties of the fabricated parts can be modulated by the SLM parameters for a fixed feedstock.

This process shows significant potential to create cellular structures with NaCl. It is also proposed that many more metal powders, such as aluminium, copper and stainless steel, which can be processed by the SLM process, will be compatible with this approach. Furthermore, other Additive Manufacturing process, such as selective laser sintering, direct metal deposition and electron beam melting process should also allow the incorporation of salt blended feedstocks to produce porous structures.

5. Conclusions

A novel technique using Ti-6Al-4V and NaCl blend to manufacture cellular structures with SLM has been demonstrated here. Both feedstock and laser build parameters were subject to experimentation. The technique for porous structure creation is shown to be repeatable and will permit new opportunities in design for a number of potential material systems. Analysis of the process and fabricated structures demonstrated the below conclusions.

- Ti-6Al-4V cubes with relative density between 0.97 and 0.51 were successfully fabricated. Increasing the volume fraction of NaCl in the feedstock resulted in increased relative density of the manufactured cubes.

- An SLM process window was defined for the range of feedstocks prepared for this study which is bounded by material response to process which results in failed builds.

- When the relative density reached 0.8, the cubes exhibited a solid-like behaviour, with

some isolated pores. With increasing NaCl, more inter-connected pores were observed in the cubes resulting in the likely removal of all NaCl and formation of an open-cellular structure. The relationship between relative density and compressive properties of the cubes was evaluated by Gibson and Ashby's scaling equations and it was shown that whilst constants differed from those reported for regular metal foams, this form of equation, with experimentally determined constants could be used to predict mechanical performance based on relative density (and hence salt ration in the feedstock) with a prescribed range.

In summary, this technique demonstrates significant potential to enhance the materials pallet for SLM processing. Other additive manufacturing process, such as direct metal deposition and selective laser sintering process, will also be expected to be compatible with this approach.

Ethics statement

This work did not involve any active collection of human or animal data and did not require ethics approval.

Data accessibility statement

Experimental data will be made available on request through University of Nottingham data respository.

Competing interests statement

The authors have no competing interests.

Authors' contributions

AC, IA and AK conceived the concept for this study. AK provided materials and materials

insight. GZ undertook experimentation (building and characterisation. All authors contributed to data analysis and writing of this manuscript. All authors gave final approval for publication.

References

1. García-Moreno, F., *Commercial Applications of Metal Foams: Their Properties and Production.* Materials, 2016. **9**(2): p. 85.

2. Osman, R. and M. Swain, *A Critical Review of Dental Implant Materials with an Emphasis on Titanium versus Zirconia.* Materials, 2015. **8**(3): p. 932-958.

3. Jha, N., et al., *Highly porous open cell Ti-foam using NaCl as temporary space holder through powder metallurgy route.* Materials & Design, 2013. **47**: p. 810-819.

4. Novák, P., et al., *High-temperature behaviour of Ti–Al–Si alloys produced by reactive sintering.* Journal of Alloys and Compounds, 2010. **504**(2): p. 320-324.

5. Augustin, C. and W. Hungerbach, *Production of hollow spheres (HS) and hollow sphere structures (HSS).* Materials Letters, 2009. **63**(13-14): p. 1109-1112.

6. Torres, Y., et al., *Development of porous titanium for biomedical applications: A comparison between loose sintering and space-holder techniques.* Mater Sci Eng C Mater Biol Appl, 2014. **37**: p. 148-55.

7. Muñoz, S., et al., *On the influence of space holder in the development of porous titanium implants: Mechanical, computational and biological evaluation.* Materials Characterization, 2015. **108**: p. 68-78.

8. Jia, J., A.R. Siddiq, and A.R. Kennedy, *Porous titanium manufactured by a novel powder tapping method using spherical salt bead space holders: Characterisation and mechanical properties.* J Mech Behav Biomed Mater, 2015. **48**: p. 229-40.

9. Aşık, E.E. and Ş. Bor, *Fatigue behavior of Ti–6Al–4V foams processed by magnesium space holder technique.* Materials Science and Engineering: A, 2015. **621**: p. 157-165.

10. Wu, J., et al., *Open-celled porous NiAl intermetallics prepared by replication of carbamide space-holders.* Transactions of Nonferrous Metals Society of China, 2011. **21**(8): p. 1750-1754.

11. Bafti, H. and A. Habibolahzadeh, *Production of aluminum foam by spherical carbamide space holder technique-processing parameters.* Materials & Design, 2010. **31**(9): p. 4122-4129.

12. Aida, S.F., et al., *Effect of NaCl as a Space Holder in Producing Open Cell A356 Aluminium Foam by Gravity Die Casting Process.* Procedia Chemistry, 2016. **19**: p. 234-240.

13. Łazińska, M., et al., *Porous graded FeAl intermetallic foams fabricated by sintering process using NaCl space holders.* Materials Science and Engineering: A, 2015. **636**: p. 407-414.

14. Mondal, D.P., et al., *The effect of the particle shape and strain rate on microstructure and compressive deformation response of pure Ti-foam made using acrowax as space holder.* Materials Science and Engineering: A, 2015. **625**: p. 331-342.

15. Wysocki, B., et al., *Microstructure and mechanical properties investigation of CP titanium processed by selective laser melting (SLM).* Journal of Materials Processing Technology, 2017. **241**: p. 13-23.

16. Mazur, M., et al., *Mechanical properties of Ti6Al4V and AlSi12Mg lattice structures manufactured by Selective Laser Melting (SLM).* 2017: p. 119-161.

17. Nagasaka, Y., N. Nakazawa, and A. Nagashima, *Experimental determination of the thermal diffusivity of molten alkali halides by the forced Rayleigh scattering method. I. Molten LiCl, NaCl, KCl, RbCl, and CsCl.* International Journal of Thermophysics, 1992. **13**(4): p. 555-574.

18. Boivineau, M., et al., *Thermophysical Properties of Solid and Liquid Ti-6Al-4V (TA6V) Alloy.* International Journal of Thermophysics, 2006. **27**(2): p. 507-529.

19. Mellin, P., et al., *Evaluating flowability of additive manufacturing powders, using the Gustavsson flow meter.* Metal Powder Report, 2017. **72**(5): p. 322-326.

20. Simonelli, M., *Microstructure evaluation and mechanical properties of selective laser melted Ti-6Al-4V.* A Doctoral Thesis, 2014.

21. Torres, Y., J.J. Pavón, and J.A. Rodríguez, *Processing and characterization of porous titanium for implants by using NaCl as space holder.* Journal of Materials Processing Technology, 2012. **212**(5): p. 1061-1069.

22. Pederson, R., *Microstructure and phase tranformation of Ti-6Al-4V.* A Doctoral Thesis, 2002.

23. Gibson, L.J. and M.F. Ashby, *Cellular Solids: Structure and Properties*. 1999: Cambridge University Press. 510.

24. Loginov, Y.N., et al., *Determining the Young's modulus of a cellular titanium implant by FEM simulation.* AIP Conference Proceedings, 2017. **1915**(1): p. 030010.
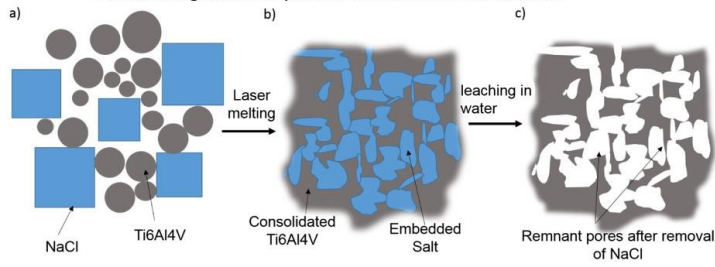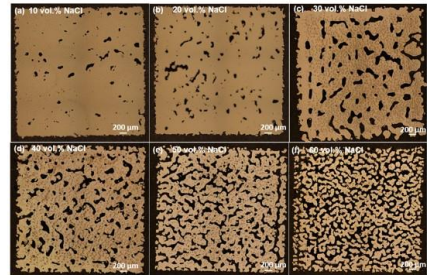
1, A new material salt based feedstock for SLM
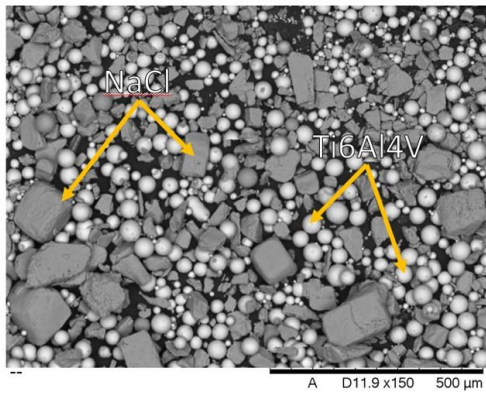
3, Processing parameters are defined
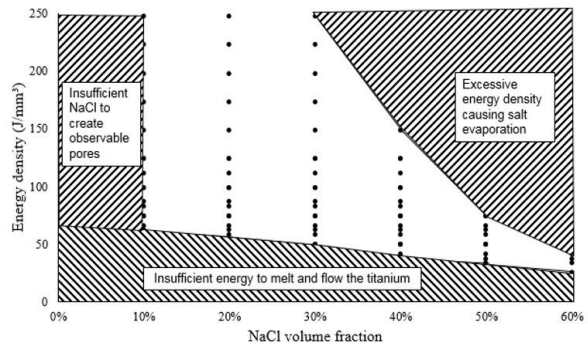
2, Leaching allows a porous structure to be created

4, Porous structures created without computational overhead

Graphical abstract

Highlights

- A new technique is reported which allows the rapid creation of porous structures via SLM using space holding methods.
- Mechanical properties of these are appraised.
- The process mechanics are explained and related to the design limits of this technique.
- The material interactions are investigated and used to propose future research opportunities in this field.